Proceedings of BS2013:
13th Conference of International Building Performance Simulation Association, Chambéry, France, August 26-28

NUMERICAL STUDY ON SPECULAR SOLAR REFLECTORS AIMED AT INCREASING SOLAR REFLECTIVITY OF BUILDING ENVELOPE

Masatoshi Nishioka[1], Craig Farnham[1], Minako Nabeshima[1], Masaki Nakao[1]
[1]Osaka City University, Osaka, Japan

ABSTRACT

Techniques that improve solar reflectivity of urban surfaces to mitigate urban heat island phenomenon have become widespread with the use of highly-reflective paints (Kondo, 2008). Since these reflective paints have a higher proportion of diffuse reflection, there is an anxiety that if used on the sides of buildings, much of the reflected solar radiation is scattered toward the ground and surrounding buildings. This becomes even more of a problem when used in narrow street canyons. Therefore, we aim to develop reflectors with the ability to direct the reflected solar radiation back to the sky.

Retroreflective surfaces are widely used in order to increase visibility of road signs at night (Woltman, 1982), because they reflect car headlights back in the direction from which they came. However, if the aim is to use retroreflectors on building envelopes for solar radiation reflection, the diurnal apparent motion of the sun makes it difficult to reflect efficiently. There was little knowledge or past research about such reflective performance, therefore we examine it in this paper.

In this research, we use corner cube retroreflectors consisting of four pieces of aluminum reflector panel with a glossy surface. At first, the reflective performance of the retroreflector consisting of ideal mirrors are evaluated by numerical simulation. Then, more realistic reflectors consists of aluminum mirrors are evaluated. The reflectivity of the mirror plate is measured by spectrophotometer and the bidirectional reflectance distribution is measured by goniophotometer. These radiant properties were used in the numerical simulation using a Monte Carlo path tracing method.

INTRODUCTION

When considering the thermal function of building exterior walls, protection of the interior space from the changing exterior climate is not their only role. They are also one of the components of the urban surface, influencing the urban heat island phenomenon.

The major role of exterior walls is to thermally isolate the interior space from the outside climate. Enhanced solar reflectance of the surface of building roof materials, called “cool-roof”, can reduce the heat load from solar radiation in the summer season. Further, in terms of heat island mitigation, absorption of solar radiation leads to an increase of convective heat to the urban atmosphere, so it is desirable to reflect away as much of the solar radiation as possible. For these purposes, cool-roof technology has become popular in recent years, and the typical application is highly reflective paint.

In order to mitigate the heat island phenomenon, the amount of solar absorption on urban surfaces should be reduced. For example, in the case of a roof surface in Fig. 1, reflection in any direction will cause no trouble. However, in the case of an urban canyon, more than half of the reflected radiation is downward and will ultimately be absorbed by the ground or lower buildings. Consequently, for the cool-roof concept to be effectively applied to walls as a heat island countermeasure, solar reflectors should be designed so that the reflected radiation is directed back towards the sky.

SURFACE TEMPERATURE DISTRIBUTION AND SOLAR RADIATION

The typical daily heat balance of an urban surface that is open to the sky is shown in Fig. 2. The latent heat component caused by moisture evaporation is disregarded for this simple expression. The heat source is solar radiation absorbed by the urban surface. The heat is dispersion has two components, heat convection to the urban atmosphere and radiation to the sky. Because the cooling and the heating on the urban surface for one day are roughly in balance, the thermal storage to the ground can be

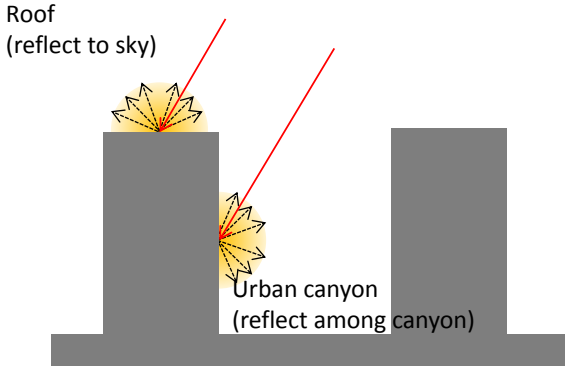

Figure 1 Overview of reflection on urban surfaces

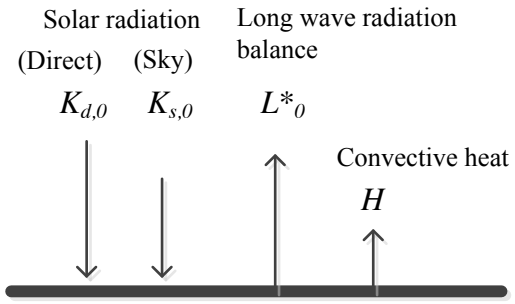

Figure 2 Daily heat balance on urban surface open to the sky

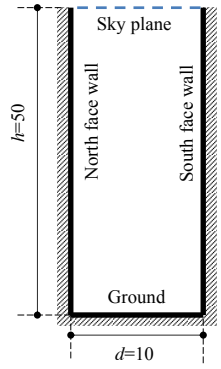

Figure 3 2D urban canyon shape with East-West axis

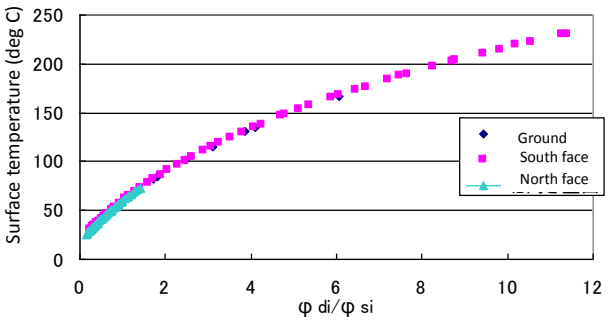

Figure 4 $\varphi_{d,i}, \varphi_{s,i}$ and daily mean surface temperature No convective heat transfer.

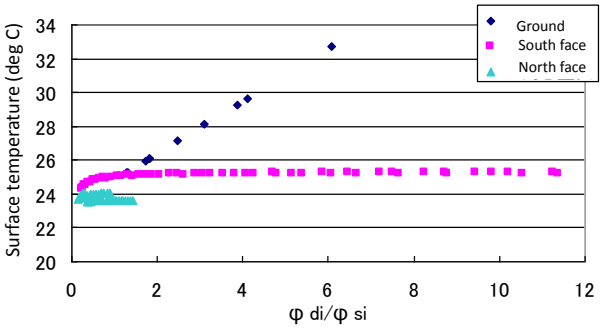

Figure 5 $\varphi_{d,i}, \varphi_{s,i}$ and daily mean surface temperature Convective heat transfer coefficient as 18 W/m^{2}K

ignored here. The formula represented by the above heat transfer is as follows.

$$K_{d,0} + K_{s,0} - L^*_0 - H = 0 \quad (1)$$

$$L^*_0 = \sigma T_s^4 - L_a \quad (2)$$

The direct solar radiation to an unshielded, open surface is $K_{d,0}$, the sky radiation is $K_{s,0}$, the balance of long-wave radiation is L^*_0 , and the heat convection is H.The Stefan-Boltzmann constant is σ , the surface temperature is T_s , and the atmospheric radiation is L_a .

However, actual urban surfaces are usually not simple horizontal planes as in Fig. 2. They are uneven and complex shapes as in Fig. 1. A more complex phenomenon is caused by complex shapes.

For the simple expression, consider the case where the heat balance is determined only by the radiation balance with the convection component is assumed to be 0 in Eq.1. The direct solar radiation incoming to the surface free of solar shielding is $K_{d,0}$, and sky solar radiation is $K_{s,0}$. However, the typical surfaces in an urban canyon are not free from solar shielding, so the two factors $\varphi_{d,i}, \varphi_{s,i}$ are introduced in Eq.3 and Eq.4. As the factors $\varphi_{d,i}, \varphi_{s,i}$ depend on the position in the urban canyon, those factors have subscript i indicating a position.

$$K_{d,i} = \varphi_{d,i} K_{d,0} \quad (3)$$

$$K_{s,i} = \varphi_{s,i} K_{s,0} \quad (4)$$

The irradiation of a plane depends on the incoming angle, so the factor $\varphi_{d,i}$ is determined by the incoming angle and the presence or absence of sunshine. The factor $\varphi_{s,i}$ for sky solar radiation is the sky view factor of the location. The heat balance equation at surface i is expressed as Eq.5.

$$\varphi_{d,i} K_{d,0} + \varphi_{s,i} K_{s,0} - \varphi_{s,i} L^*_0 = 0 \quad (5)$$

The surface temperature is expressed as Eq.6 , derived from Eq.2 and Eq.5.

$$T_s = \left(\frac{K_{s,0} + L_a}{\sigma} + K_{d,0} \frac{\varphi_{d,i}}{\varphi_{s,i}} \right)^{1/4} \quad (6)$$

In the case of no direct solar radiation, the right-hand side of Eq.6 is free from the factors $\varphi_{d,i}, \varphi_{s,i}$, therefore the temperature at shielded surfaces and the temperature at unshielded surfaces will be equal. Therefore, it is the second term in the right-hand side of Eq.6 which determines the temperature distribution on the urban canyon surface.

A numerical simulation performed for the case of clear model solar conditions on 21,Jun in Osaka

(latitude: 34.7N, longitude: 135.5E) was performed for the urban canyon with the shape are shown in Fig. 3. Fig. 4 shows the surface temperature distribution calculated by Eq.6 under the condition of no convection. Solar radiation is set for June 21 with clear sky. Surface material is 150mm thick concrete with fully-insulated back side. Solar absorptivity and emissivity are both set to 1. The results are reasonable considering that heat dissipation through convection is not included. Though Fig. 4 is an unrealistic thought experiment, Fig. 5 shows more realistic condition, with a convection heat transfer component included. The convective heat transfer coefficient is set to 18 W/m^2K , with an atmosphere temperature varying over the range 23.5 +/- 4 deg C. In the ground temperature distribution, the same trend as Fig. 4 is shown, although the effect on temperature of North-face wall and South-face wall is slight, because the solar radiation is very little.

As described above, the surface temperature distribution is governed by the second term of right-hand side of Eq.6 Therefore, if the direct solar radiation can be reflected to the sky, rather than to other canyon surfaces, the surface temperature in urban canyon will be decreased.

RETROREFLECTOR

A directive reflector is made with a specularly reflective material. The direction of reflection can be controlled to account for the sun position depending on the time and season. By automatically controlling a motorized mount, the mirror facing can direct solar radiation as desired. However, a means to control the direction of reflection without using a movable mechanism is desirable from the viewpoint of cost.

Overview of retroreflector

Given the issues mentioned above, the authors have focused on a retroreflector. Retroreflection is the phenomenon of light rays striking a surface and reflecting back along the same path to the source of the light. A retroreflector can do this without using a movable mechanism, just by the nature of its structure. It is an ideal reflector for the sun for our purpose, sending solar radiation back to the sky regardless of the solar position. The solar radiation reflective characteristics of the retroreflector shown in Fig. 6(a) is discussed in this section. The reflector unit consists of four mirrors (Mirror I - IV). These units are arranged in a reflector array (Fig. 6(b)) which consists of multiple reflector units, each of several centimeters scale.

Fig. 7(a) illustrates the typical paths through which reflection occurs in this unit. Retroreflection occurs when the path of light reflects 3 times, on three pieces of mirror. It can also occur with paths having 5 or more reflections when incoming on an angle as in Fig. 7(b). In case of one or two reflections, reflection will generally not go back to light source. We call these cases “Non-retroreflection”.

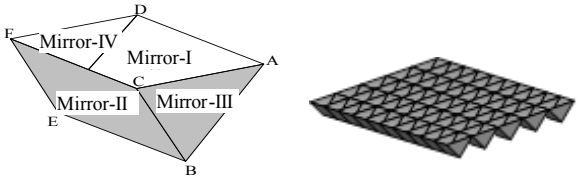

(a) Reflector unit (b) Reflector array

Figure 6 Overview of retroreflector

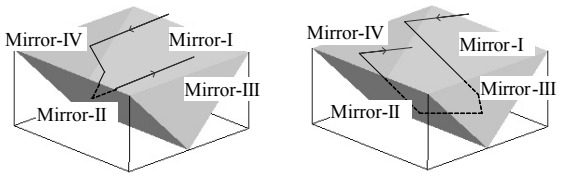

(a) Reflection 3 times (b) Reflection 5 times

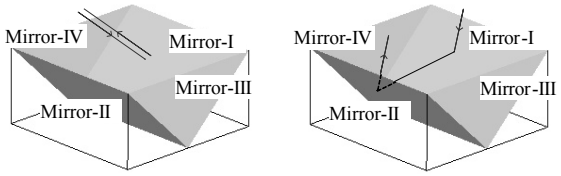

(c) Reflection 1 time (d) Reflection 2 times

Figure 7 Typical 4 paths of reflection in retroreflector unit

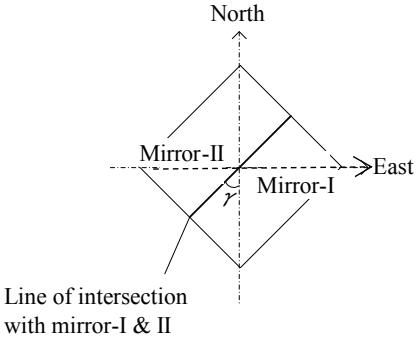

(a) Azimuth angle γ

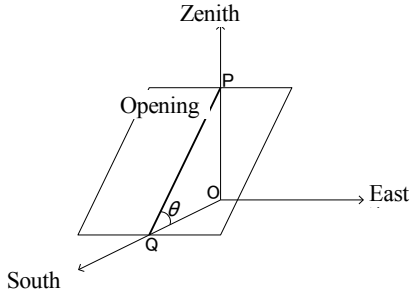

(b) Tilt angle θ

Figure 8 Definition of installation angle

Reflective characteristics of retroreflector consisting of ideal mirrors

The amount of reflection for 9 cases of installation angle of a retroreflector are discussed in this section.

Numerical simulation by Monte Carlo path tracing method (MPT) was performed on one representative day (the 21st) for each month. The geometric calculations done in the simulation used CGAL (Computational Geometry Algorithms Library). Each mirror in the retroreflector is assumed as an ideal mirror. The sun position is calculated for Tokyo (latitude: 35.7N, longitude: 139.8E). Installation angles are defined in Fig. 8.

Direction of reflection is classified into 3 types; retroreflection, reflecting to the angle within 22 degrees from zenith, and reflecting to the angle within 22 to 39 degrees from zenith. The fraction of the retroreflector area yielding each type is shown in Fig. 9 and Fig. 10 (Nishioka et al. 2008). The retroreflective component is the component toward the sun position, and two other types inside of the angles from the zenith are called "Effective reflection area", in that the reflection most likely will reach the sky without hitting any other buildings. The zenith angles are determined by referring to the set-back line regulation based on Japanese Building Standards. In the three months of the summer season (Fig. 9), 70% of the reflection is included in the "Effective reflection area" in the case of the best installation angle(γ =90 degrees , θ =15 degrees). As the configuration factor from a horizontal plane to "Effective reflection area" is about 40%, the effective reflection is 1.75 times that of the reflection in the case of typical diffuse reflection.

DIRECTIVE REFLECTOR SIMILAR TO THE RETROREFLECTOR

The results in the previous section show the superiority of retroreflector compare to diffuse reflector in the reflective performance toward the sky. However, the structure of the reflector often requires 3 or more reflections to redirect incoming sunlight back to the sky. This makes it difficult to obtain high reflectivity. For example, if the retroreflector is made of a material with a reflective index of 0.9, the net reflectivity after 3 reflections is reduced to $(0.9)^3$=0.73.

In this section, rather than focus on retroreflection, we examine the amount of light reflected back to the sky by a directional reflector. To analyze the reflectance characteristics of commonly used reflective material, the Bidirectional Reflectance Distribution Function (BRDF) of commercial reflective aluminum panels was measured. Then, the inputs of a parametric reflection model are adjusted to match the measured values. These parameters and the model are then used in a reflectivity simulation to estimate the reflective characteristics of a reflector made from several panels of the previously measured reflective material.

IDENTIFICATION OF BRDF PARAMETERS

The parameters required to calculate BRDF using a modified Phong BRDF model as shown in Eq. 7 are explained here. A goniophotometer is used to measure the radiance factor at regular intervals of angle of reflection. From this data, the BRDF can be calculated in Eq. 7 (Lewis 1994). Here the BRDF is ρ, the diffusive reflectivity is k_d, the specular reflectivity is k_s, the angle halfway between the perfect specular reflective direction and the outgoing direction is α, and the Phong parameter is n.

Separately, the spectral reflectivity is measured with a spectrophotometer. The values of spectra for standard sunlight as determined by Japan Industrial Standards-K in Standard JISK-5602 are applied to the measured reflectivity values to yield the expected reflectivity for sunlight, $k_d + k_s$. With this data, the only remaining unknown in Eq. 7 is the specular exponent or "Phong parameter" of n. The least-squares method is used to find the best value of n. The measured values of BRDF for reflectors made of the reflective aluminum panels and the results of the calculations using the modified Phong model are

$$\rho = k_d \frac{1}{\pi} + k_s \left(\frac{n+2}{2\pi} \cos^n \alpha \right) \tag{7}$$

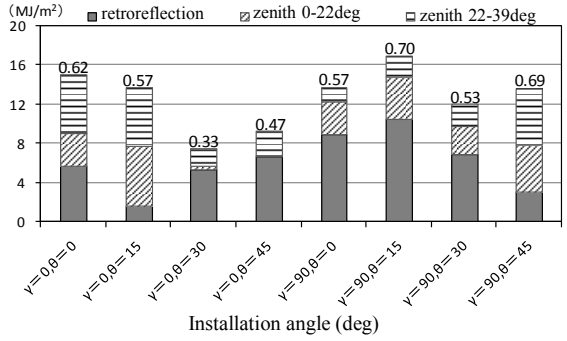

Figure 9 Three months mean reflection (Jun, Jul., and Aug.)

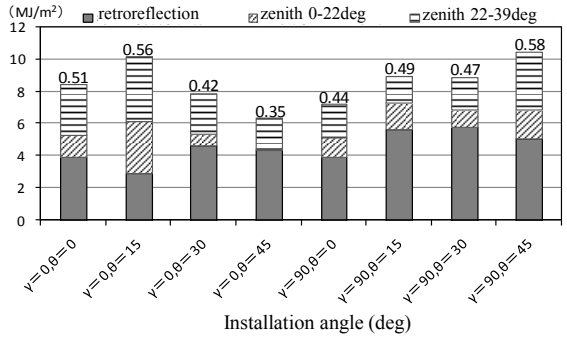

Figure 10 Annual mean reflection

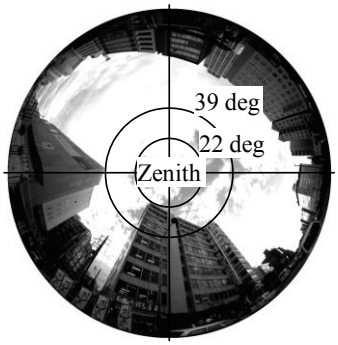

Figure 11 Zenith angle and sky view

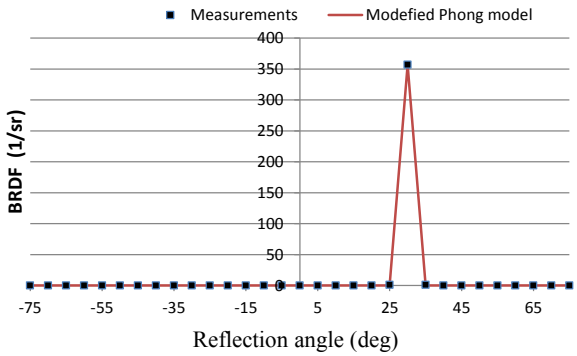

Figure 12 Measurement results and estimation by Phong model. Identified parameters: $k_d + k_s$= 0.78, n= 3137

Table 1 Measurement instruments

Instruments	Specification
Spectrophotometer	UV-3600 (Simadzu CO.LTD.) Wave length 185-3300 nm Resolution 1 nm
Goniophotometer	GCMS-4(Murakami Color Lab.) Wave length 390-730 nm Resolution 10 nm

shown in Fig. 12. The measurement equipment used is detailed in Table 1. The goniophotometer used here had the light source set at an incident angle of 30 degrees, and the measurements taken at 5 degree intervals over the span of +/-75 degrees.

The commercial reflective aluminum panels chosen for the study are typically used in solar concentrators for solar electric power, having very high specular reflectivity for an outdoor-use material. The model parameters for this material were determined to be a diffusive reflectivity of 0.07, a specular reflectivity of 0.71, and specular exponent n as 3137. For details please refer to Reference 4.

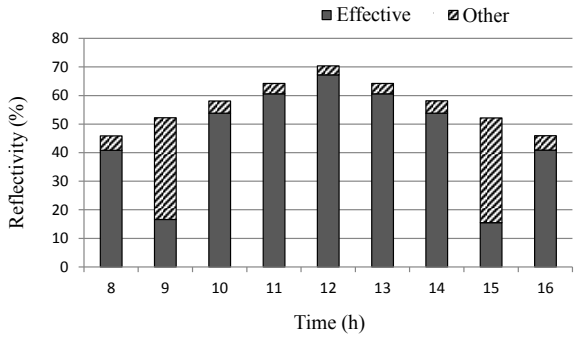

Figure 13 Reflectivity in the effective reflection field

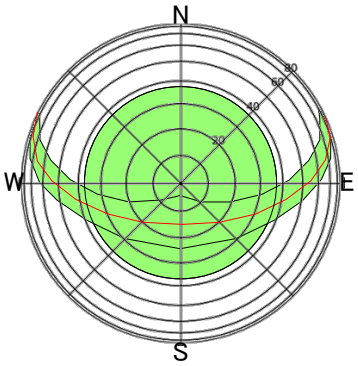

Figure 14 Field of effective reflection on the sky hemisphere

REFLECTIVITY OF DIRECTIONAL REFLECTOR

The above BRDF parameter model is used in the Monte-Carlo path tracing simulation (Lafortune 1994) to determine the reflectivity.

The directional reflector shape is set to be the same as the retroreflector shown in Fig. 6, but the single reflection case shown in Fig. 7(a) the orientation of the unit is set to only the angle ($\gamma = 90$ degrees, $\theta = 60$ degrees) at which the sunlight is strongest in summer. The reflectivity of the unit is shown in Fig. 13. However, most of the reflections in this case are 1-time reflection or 2-time reflections.

The field of effective radiation is shown in Fig. 14. It includes the area around the zenith, as well as a band including +/- 5 degrees within the path of the sun. At this unit orientation angle, retroreflection will be rare, so there is a possibility that the reflectance to the effective reflection area will be lower, but also means the number of 3-time reflections will also be low, such that the strong adverse effect on total reflectivity due to multiple reflections is largely avoided.

The reflectivity measured in section 4.1 (specular plus diffuse) is 0.78, so the reflectivity of a 3-relfection case becomes 0.47. This is about half of

the value calculated for the case of the ideal reflector discussed in Section 3.2. However, by installing the reflector at an incline such that 1-reflection cases dominate, the reflectivity to the effective reflection area of the sky can be as high as 40%-60%.

CONCLUSIONS

This paper examined the potential for the effectiveness of using directional reflectors on building surfaces to reflect sunlight back to the sky. Further, to illustrate the effect, case studies were made through a numerical simulation, yielding the reflectivity characteristics of the directional reflectors. When installing such reflectors on actual building surfaces, it will be necessary to take steps to counter the reflective glare, but this is a solvable problem. The day when directional reflectivity is included in the design phase of building exteriors may not be long off.

NOTE: To simplify the heat balance in the explanations, the surface solar absorptivity and the long wave radiation diffusivity are both set to 1. Also, the long wave radiation is taken as only the exchange between the urban surface and the sky. Mutual exchange between urban surfaces is ignored.

REFERENCES

CGAL, Computational Geometry Algorithms Library, http://www.cgal.org

JIS K 5602, 2008, Determination of reflectance of solar radiation by paint film

Kondo, Y., Ogasawara, T., Ohki, T., Udoh, K., 2008, Reduction of sensible heat emission by increasing roof solar reflectance as a countermeasure of heta island phenomena, Architectural Institute of Japan; No.629, pp.923-929, in Japanese

Lafortune, E. P., Willems, Y. D., 1994. Using the modified Phong reflectance model for physically based rendering, Technical Report CW197, Dept. Comp. Sci., K.U. Leuven

Lewis, R. R. 1994. Making shaders more physically plausible. Computer Graphics Forum, Vol. 13, pp.109-120

Nishioka, M., Inoue, S., Nakao, M., Nabeshima, M., 2008. Numerical simulation on basic properties of retroreflectors, Journal of Environment Engineering, Architectural Institute of Japan; No.630, pp.1013-1019, in Japanese

Woltman, H., 1982, Use of retroreflectors in the improvement of nighttime highway visibility, Color Research & Application, Vol. 7, pp. 247–251